Rare Met. (2024) 43(8):3913–3920
https://doi.org/10.1007/s12598-024-02715-8

RARE METALS

ORIGINAL ARTICLE

Oxidation behavior of Ni-based superalloy GH4738 under tensile stress

Ji-Chong Hu, Hai-Liang Huang, Chong-Chong Wu, Xiao-Yu Sun, Jie Wang, Yan-Hong Yang, Jing-Long Qu, Liang Jiang, Jin-He Dou, Yang Chen*

Received: 11 October 2023 / Revised: 4 December 2023 / Accepted: 4 December 2023 / Published online: 14 May 2024

Abstract Revealing the oxidation behavior of superalloys is crucial for optimizing material properties and extending service life. This study investigated the oxidation behavior of superalloy GH4738 under stress states at 850 °C. High-throughput specimens were fabricated to withstand different stresses at the same time. Isothermal oxidation samples were analyzed using the mass gain method to obtain oxidation kinetic curves. The results show that the external stress below 200 MPa could improve the oxidation resistance of the GH4738. With tensile stress increasing, the oxide layer becomes thinner, denser and more complete, while internal oxidation decreases. The tensile stress alters the structure of the external oxide layer from a two-layer to a three-layer configuration. The Cr_2O_3 oxide layer inhibits the outward diffusion of Ti, leading to Ti enrichment at the oxide–matrix interface and altering the oxidation mechanism of GH4738.

J.-C. Hu, H.-L. Huang, C.-C. Wu, J. Wang, L. Jiang, Y. Chen*
Institute for Advanced Studies in Precision Materials, Yantai University, Yantai 264005, China
e-mail: chenyang@ytu.edu.cn

X.-Y. Sun
Department of Management and Engineering, Linköping University, 58183 Linköping, Sweden

Y.-H. Yang
Shi-Changxu Innovation Center for Advanced Materials, Institute of Metal Research, Chinese Academy of Sciences, Shenyang 110016, China

J.-L. Qu
Gaona Aero Material Co.,Ltd, Beijing 100081, China

J.-H. Dou
College of Artificial Intelligence and Big Data, Shandong First Medical University and Shandong Academy of Medical Sciences, Jinan 250117, China

Keywords Ni-based; Superalloy; Oxidation behavior; Tensile stress; Oxide layer

1 Introduction

GH4738, a precipitation-hardened superalloy, possesses excellent oxidation resistance, corrosion resistance and superior creep strength at high temperature, which is widely used in aerospace, petrochemical and power generation fields [1–3]. Harsh service environments can lead to severe oxidation, consuming alloy-strengthening elements and initiating microcracks, thereby weakening mechanical properties and shortening the service life of superalloy [4–6]. Furthermore, the interaction between external stress and superalloy oxidation is complex and controversial [7, 8].

Previous studies focused on the high-temperature mechanical properties and microstructure of GH4738, such as creep [9–11], fatigue crack extension and structural stability [12–14]. Ma et al. [15] employed room temperature machining (RTM) and low-temperature burnishing (LTB) surface treatment techniques to improve the microstructure of GH738 superalloy. The results proved that nanograins and higher twins density generated on LTB specimen triggered the formation of protective Al_2O_3 layer, thereby inhibiting the diffusion of elements and significantly improving oxidation resistance of specimen. Wang et al. [16] investigated the oxidation behavior of GH738 in static air between 800 and 1000 °C for 100 h, and believed that the oxidation process was controlled by the diffusion of alloying elements in metal matrix and chromia. However, the oxidation behavior of GH4738 under stress still needs systematic and embedded investigation.

Table 1 Measured chemical composition of GH4738 (wt%)

Cr	Co	Mo	Al	Ti	C	B	Zr	Ni	Fe	Mn	P	S	Si
18–21	12–15	3.5–5.0	1.20–1.60	2.75–3.25	0.02–0.08	0.003–0.01	0.02–0.08	Bal.	≤ 2.0	≤ 0.1	≤ 0.015	≤ 0.015	≤ 0.15

Owing to the coupling effects of multiple elements in superalloys, the oxidation mechanism under different external stress would be complex. Some researches proved that the tensile stress would aggravate the oxidation. Zhou et al. [17] proved that both the applied tensile stress and compressive stress would diminish the oxidation resistance of pure Ni during 20 h of oxidation at 973 K, and the effect of the compressive stress was more significant. Ramsay et al. [8] verified that tensile stress accelerated the internal oxidation of RR1000 under 900 MPa at 700 °C, which was consistent with the stress-assisted grain boundary oxidation (SAGBO) phenomenon, and a verification model had been developed. Ma et al. [7] applied 330 MPa to the single-crystal superalloy at 1150 °C and found that the diffusion of Al increased, leading to an increase in oxidation rate. However, several researchers found that stress could improve the oxidation resistance of superalloys under specific circumstances. Ye et al. [18] applied different small tensile stresses on the novel powder metallurgy superalloy at 900 °C, while the results showed that the internal oxidation decreased with pressure. At the same time, the external stress would hinder the outward diffusion of Ti. Similarly, the oxidation behavior of DZ125 under 100 MPa at 980 °C showed that the oxidation rate decreased with the increasing applied pressure [19].

The above researches indicate that although the interaction between oxidation and external stress at high temperatures has received extensive attention, the coupling effects of the oxidation temperature and tensile stress on the oxidation behavior of superalloy have not been systematically studied. The corresponding oxidation mechanism has not been deeply investigated. In this study, the oxidation experiments of GH4738 superalloys under different tensile stresses at 850 °C were carried out. The influence of external pressure on oxidation behavior and mechanism of GH4738 was analyzed in detail, which would contribute to the development of superalloys servicing under harsh environment.

2 Experimental

GH4738 alloy, provided by Wuxi Paike New Materials Technology Co., Ltd., with the chemical composition shown in Table 1, was used in this study. The samples were cut into 30mm × 10mm × 2 mm slices for the subsequent experiment. The surface of the samples was ground with metallographic sandpaper up to 2000 mesh. The

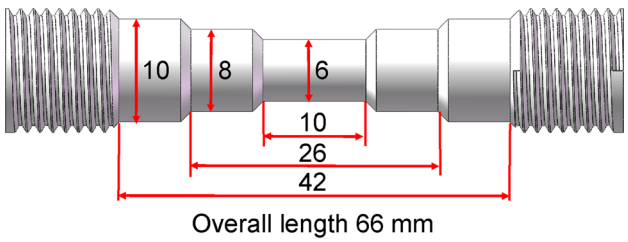

Fig. 1 Shape and size of high-throughput specimen under tensile stress (unit: mm)

samples were polished and ultrasonically cleaned in ethanol. After drying, the samples were measured in detail with an electronic Vernier caliper.

Before the oxidation experiment, the pristine corundum crucibles underwent drying at 50 °C, a temperature above the predetermined experimental temperature, until a constant mass was achieved. Subsequently, the samples were weighed and placed into the high-temperature chamber furnace (Nabertherm GmbHN11/H) to conduct the isothermal oxidation experiment. To minimize temperature errors, an external thermocouple was employed for temperature correction before each experiment. The oxidation experiments were conducted at 850 °C for varying durations of 1, 5, 10, 25, 50 and 100 h, respectively. An electronic scale with an accuracy of 0.01 mg was utilized to measure the sample's weight before and after the oxidation experiment. The oxidation weight gain per unit area was then calculated based on the sample's weight gain and surface area to generate the oxidation kinetic curve. The composition, surface and cross-sectional morphologies of the oxide film were analyzed using X-ray diffractometer (XRD, MiniFlex600/600-c, Rigaku), tungsten filament scanning electron microscope (SEM, VEGA, Tescan) and focused ion beam-scanning electron microscope (FIB-SEM, Amber, Tescan).

The GH4738 superalloy, supplied by Fushun Special Steel, underwent mechanical processing to form a 66 mm high-throughput stepped axial tensile sample, as illustrated in Fig. 1. This design allows a single sample to withstand different stresses in the same state. Following manufacturing, the samples were ultrasonically cleaned in ethanol and dried. Subsequently, the samples were oxidized for 50 h at 850 °C under constant tensile stress, with real stresses of 200, 112.50 and 72.00 MPa at the center of cylinders with a diameter of 6, 8 and 10 mm, respectively. The samples were heated to the specified temperature and loaded with target pressure. After being oxidized for 50 h

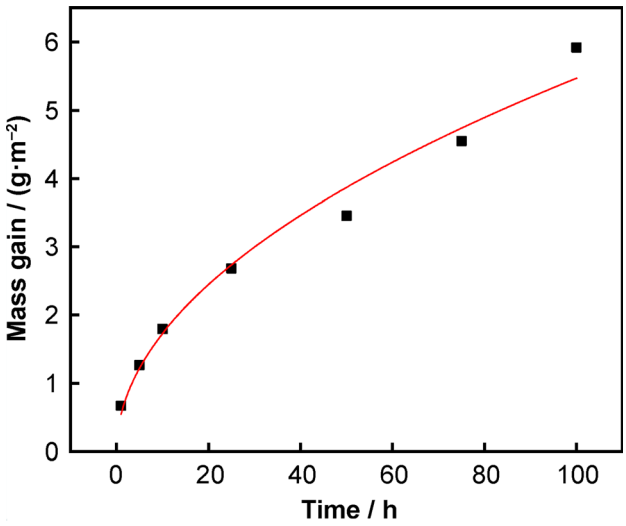

Fig. 2 Oxidation kinetic curve of GH4738 at 850 °C

under constant tensile stress, the samples were unloaded and air-cooled. The composition, structure and morphology of the oxide film were analyzed by XRD and SEM.

3 Results and analysis

3.1 Oxidation kinetics

Figure 2 illustrates the oxidation kinetic curve of GH4738 alloy in static air at 850 °C for 100 h. Figure 2 shows that the oxidation kinetic curves of the samples at 850 °C primarily followed the parabolic law. The kinetic curve reveals a rapid mass gain during the initial oxidation stage, a gradual slowdown with extended oxidation time, and eventually reaches a relatively stable stage.

Previous studies indicate that the oxidative mass gain over time can be approximately expressed as Eq. (1) [20, 21]:

$$(\Delta m/A)^2 = k_p t \quad (1)$$

where $\triangle m$ is the oxidative mass gain, A is the surface area of the sample, k_p is the oxidation parabolic rate constant and t is the oxidation time.

Analyzing the oxidation kinetic curves provides insights into the alloy's behavior at different stages of the oxidation process [22, 23]. Initially, chemical and physical combination of oxygen and alloy matrix elements occurs, leading to the nucleation of defects such as grain boundaries and dislocations on the alloy surface, forming an oxide film. The oxide growth rate is rapid during this stage. With increased oxidation time, the curve gradually slows down, indicating a transition from interface reaction control to an element diffusion mechanism due to the continuous formation of a compact and continuous oxide film.

3.2 Analysis of oxidation products

XRD patterns of GH4738 oxidized at 850 °C with no stress and under different tensile stresses are presented in Fig. 3. GH4738 exhibits a distinct oxidation pattern at 850 °C. XRD patterns in Fig. 3a demonstrate changes in the peak strength of oxidation products over time. Oxides such as Cr_2O_3, Al_2O_3 and TiO_2 were generated at 850 °C. With the extension of oxidation, the peak strength of the matrix decreased, while the peak value of the oxide increased, indicating that the thickened oxide layer gradually covers the matrix.

The effect of tensile stress on the phase structure of GH4738 after 50 h oxidation is shown in Fig. 3b. A new phase $NiCr_2O_4$ generates under stress, and the diffraction peaks of various oxidation products become more prominent. Increased tensile stress results in weaker diffraction peaks of oxides and a stronger matrix, attributed to a thinner oxide layer.

3.3 Morphology and composition analysis of oxides

Figure 4 displays the isothermal oxidation surface morphology of GH4738 at 850 °C for 100 h. Figure 4a reveals the formation of a thick, continuous oxide film on the sample surface, with more severe oxidation in grain boundary areas than intragranular regions. No obvious defects such as cracks, micropores and oxide spalling are observed. The oxidation products are relatively simple, and the primary oxidation products are irregular spherical (Fig. 4b) and granular (Fig. 4c) particles. Combined with the data in Table 2, the irregular spherical particles are TiO_2. As shown in region II (Fig. 4c), the oxide products are dense, uniform and irregular particles. The results in Table 2 demonstrate that the granular particles are mainly composed of titanium oxide and chromium oxide, which is consistent with XRD results. The extremely low content of Ni indicates that the oxide layer thickens. The strong adhesion between the oxide film and the substrate is evidenced by the absence of apparent peeling of the oxide layer at 850 °C.

3.4 Cross-sectional morphology and composition of samples under constant stress

Figure 5 depicts the cross-sectional morphology structure and element distribution of GH4738 oxidized at 850 °C for 50 h under different stresses. Internal and external

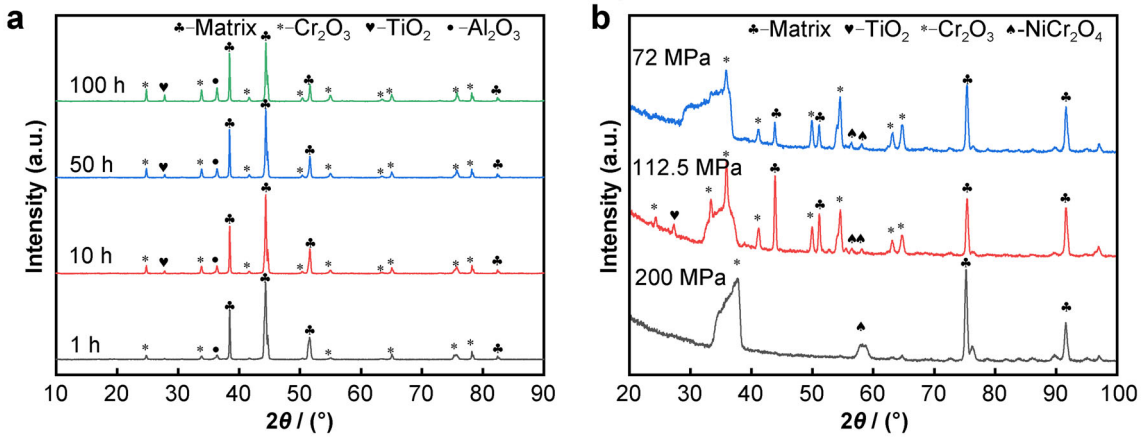

Fig. 3 XRD patterns of GH4738 oxidized at 850 °C with **a** no stress and **b** tensile stress

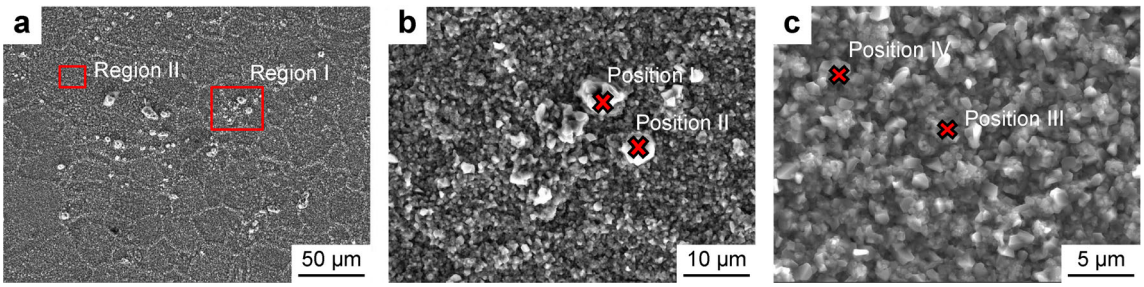

Fig. 4 **a** Surface morphology of GH4738 oxidized at 850 °C for 100 h; magnification of **b** Region I and **c** Region II

Table 2 Compositions of oxides in Fig. 4 after oxidation tests at 850 °C for 100 h (at%)

Position	O	Ti	Cr	Al	Ni
I	66.1	31.0	1.9	0.2	0.5
II	58.7	38.2	2.2	0.2	0.4
III	59.0	4.8	34.3	0.5	1.4
IV	63.6	17.9	17.3	0.3	0.9

oxidation zones of samples under different states are distinguished by the interface between oxides and the superalloy matrix. As shown in Fig. 5a, the internal oxidation products are discrete or semi-continuous. A portion of internal oxides extend into the metal matrix along the grain boundary of about 4 μm. Compared with the samples under constant stress, the structure of the external oxidation is relatively simple. As shown in Fig. 5a, the external oxides are divided into two sections, an outermost dark gray Ti-rich layer and a light gray CrTi-rich layer adjacent to the metal matrix with thickness of ~ 2 μm. The oxide composition perpendicular to the interface direction was analyzed by energy-dispersive spectrometer (EDS) (Fig. 5a). Combined with XRD patterns, the oxides of the outermost layer I are supposed to be TiO_2, and the composition of the inner layer II is Cr_2O_3 and TiO_2. The surge of Ni content distinguishes the metal matrix from the outer oxide scales. The peaks of Al and Ti contents indicate the inner oxidation diffusion.

The external oxidation structure of samples under stress, which is different from the samples without stress, contains three layers (Fig. 5b–d). The outermost non-continuous dark gray layer I was determined as TiO_2 based on XRD and line scanning analysis. The subouter thick light gray layer II was mainly composed of Cr_2O_3 and TiO_2. The inner oxide scale III contained a large amount of Ni, Ti and O and a small amount of Cr, which was supposed to be $NiCr_2O_4$ and TiO_2 according to XRD results. In the internal oxidation region IV, the Al_2O_3 oxides extended into the metal matrix, diffusing uniformly and continuously along the grain boundary. Interestingly, with the increase in the stress, the thickness of the oxide layer decreased from 15.25 to 7.67 μm.

Combined with the comparative data under four different stress states, as the tensile stress increased, the micropores in the external oxide film decreased unexpectedly (Fig. 5), indicating a decrease in the compressive stress inside the oxide films [18]. The increasing tensile stress contributed to the formation of dense and continuous Cr_2O_3 oxide film, which effectively prevented the mutual diffusion of metal elements and oxygen. This can be verified by the reduced external oxide layer thickness and internal

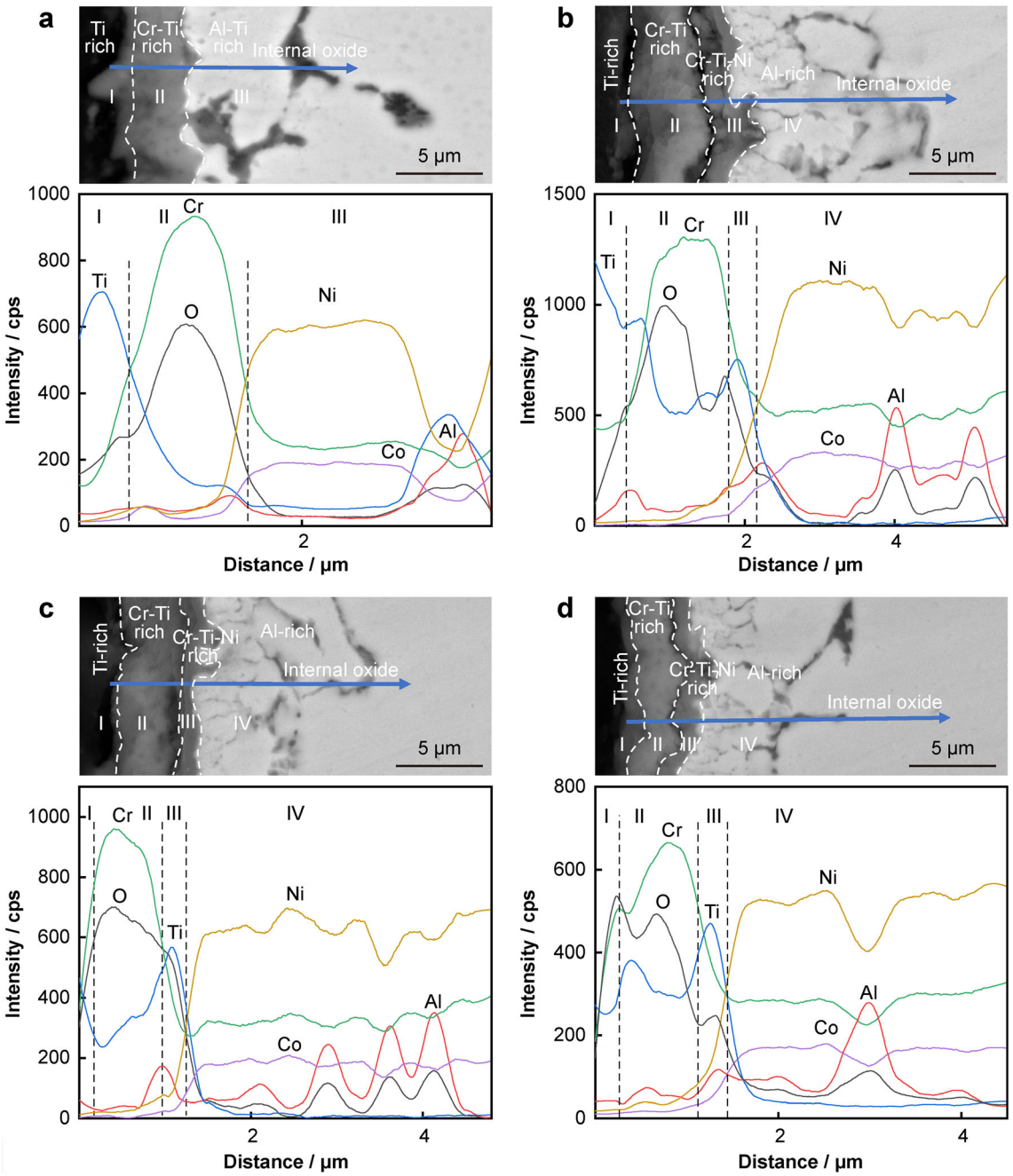

Fig. 5 Cross-sectional morphology and element distribution of GH4738 oxidized at 850 °C for 50 h under **a** 0 MPa, **b** 72 MPa, **c** 112.5 MPa and **d** 200 MPa

oxidation depth, as shown in Fig. 6, indicating improved oxidation resistance through external tensile stress.

4 Discussion

Based on the aforementioned findings, it can be inferred that an increase in tensile stress (0–200 MPa) enhances the oxidation resistance of GH4738 superalloy. Moreover, stress impedes the diffusion of Ti through the Cr_2O_3, leading to the accumulation of more Ti beneath the Cr_2O_3 oxide layer.

The schematic illustration of the oxidation mechanism, with and without stress, is shown in Fig. 7. External force altered the structure of the external oxide layer from TiO_2 + CrTi-rich oxide to TiO_2 + CrTi-rich oxide + NiCrTi-rich oxide configuration. The internal oxides shifted from Al/Ti-rich oxide to Al_2O_3. The thickness of the

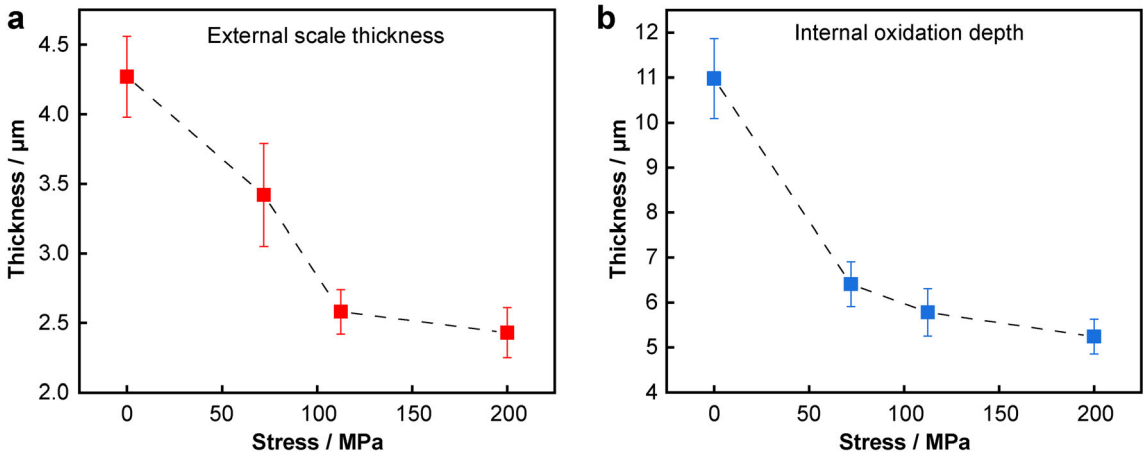

Fig. 6 External oxide scale thickness and internal oxidation depth of GH4738 after oxidation at 850 °C for 50 h under different stress states

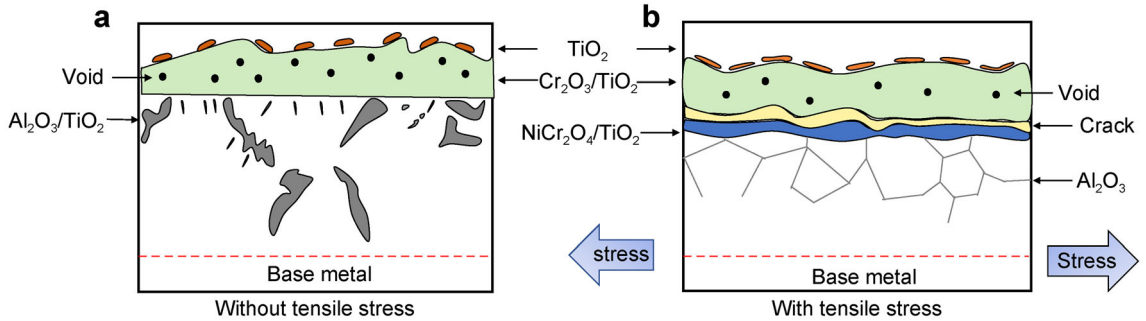

Fig. 7 Schematic illustration for oxidation mechanism of GH4738 **a** without and **b** with tensile stress

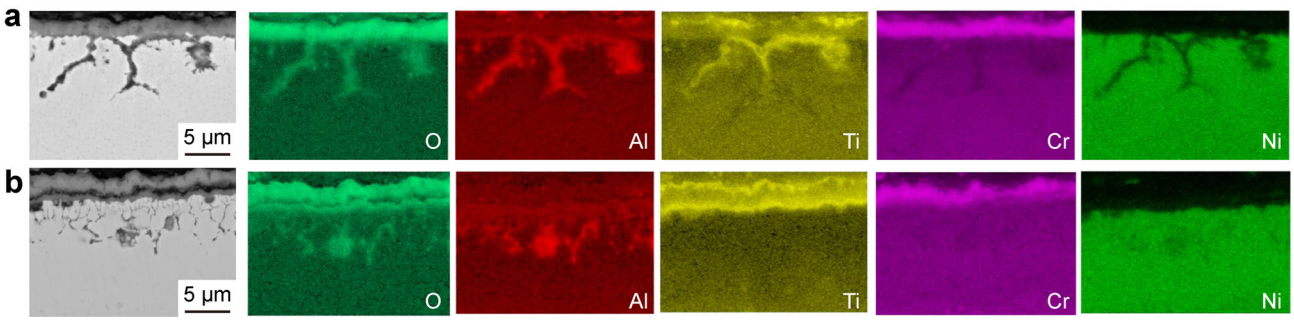

Fig. 8 Cross-sectional elements distribution of GH4738 oxidized at 850 °C for 50 h under **a** 0 MPa and **b** 200 MPa

external oxide film and the depth of the internal oxidation decreased with increasing tensile stress from 0 to 200 MPa. These above results confirmed the positive effect of tensile stress on the oxidation resistance of GH4738 within the 200 MPa range.

The cross-sectional elements distribution of GH4738 oxidized at 850 °C for 50 h under 0 and 200 MPa is shown in Fig. 8. As shown in Figs. 5 and 8, regardless of the presence of stress, Ti always appears in the outermost layer and Cr is located in the secondary outer layer. As Cr_2O_3 is a P-type semiconductor oxide, cations are mainly transferred through the oxide layer to the oxide/air interface to react with oxygen [24]. The high diffusion rate of Ti led to the formation of discrete TiO_2 particles in the outermost layer [25]. Ti-rich oxides generated adjacent to the metal matrix under stress. The external stress increased the dislocation density, thereby facilitating ion diffusion, and elevating oxygen vacancy concentration, which

significantly contributed to the formation of Cr_2O_3 layer [26]. As the applied tensile stress increased, the micropores in the oxide layer became less and smaller, which meant the oxide layer got denser. Continuous dense Cr_2O_3 oxide film effectively prevented the outward diffusion of Ti, and the diffusion rate of Ti in Cr_2O_3 oxide layer was slower than that in metal matrix, thereby resulting in accumulation of Ti beneath the Cr_2O_3 layer. Furthermore, the thickness of the external oxide scale decreased, due to that the continuous dense Cr_2O_3 oxide layer effectively inhibited the reaction of metal elements with oxygen, therefore elevating the oxidation resistance of the samples.

As shown in Fig. 5, the interface (samples under stress) between the external oxides and metal matrix exhibits wavy morphology and cracks. The phenomenon is mainly attributed to the presence of the spinel phase and TiO_2 in the innermost oxidation layer adjacent to the matrix. The volume ratio of metal atoms to oxide molecules, known as the Pilling–Bedworth ratio (PBR), for TiO_2 and $NiCr_2O_4$ is > 1. Therefore, internal compressive stress existed in the oxide layers. Additionally, the growth of the oxide layer itself, coupled with the difference in thermal expansion between the alloy substrate and the oxide film, led to the offsetting of part of the compressive stress in the oxide film against specific external forces. Excessive stress resulted in the observed wavy morphology [27, 28].

In summary, during the creep stretching process at high temperatures, the initial applied tensile stress primarily served to counterbalance the compressive stress present in the oxide layers. This allowed the oxide layer to withstand a certain amount of tensile stress, ensuring its growth in parallel with the matrix under relatively low stress. However, once the elastic strain energy in the oxide film surpassed the fracture resistance between the alloy and matrix, the oxide film would flake off. Furthermore, as oxidation progressed, the effective cross-sectional area of the sample decreased, causing the actual stress value of the matrix to exceed the theoretical stress value. The increasing tensile stress accelerated the formation of microcracks and spalling of oxide scales.

The main oxidation product of internal oxidation was Al_2O_3. It is proved that when the Cr/Al ration is high, Al_2O_3 mainly presents as an internal oxide. Only when the Al content exceeds 3 wt%, an Al_2O_3 protective layer would form in the external oxide layer [29]. As shown in Fig. 5, with increasing tensile stress, the depth of internal oxidation decreases. The diffusion rate of Cr accelerated due to the increasing stress, resulting in the rapid formation of protective chromium oxide layer. The dense Cr_2O_3 oxide layer effectively prevented the permeation of oxygen into metal matrix, thereby reducing the depth of internal oxidation [30].

5 Conclusion

High-throughput oxidation experiments were conducted on GH4738 superalloy under varying stresses at 850 °C for 50 h. The results showed that the tensile stress had great impact on the oxidation resistance of the superalloys, and the conclusions were drawn as following: The application of constant tensile stress reduced internal stress within the oxide film and induced structural changes in the film. As the tensile stress increased, the diffusion rate and dislocation of elements also rose, resulting in the rapid formation of protective Cr_2O_3 layer, and thus, in turn, contributed to a reduction in the oxidation rate. Under constant tensile stress, the rapid formation of Cr_2O_3 layer effectively impeded the outward diffusion of Ti, resulting in the accumulation of Ti beneath the Cr_2O_3 layer.

Acknowledgements This work was financially supported by the National Key R&D Program of China (No. 2021YFB3700401), Shandong Provincial Natural Science Foundation for Youths (No. ZR2022QE234), Zhejiang Provincial Natural Science Foundation (No. LQ21E030002) and the Youth Innovation team Project of Higher Education Institutions in Shandong Province (No. 2022KJ272).

Declarations

Conflict of interests The authors declare that they have no conflict of interest.

References

[1] Pillai R, Chyrkin A, Quadakkers WJ. Modeling in high temperature corrosion: a review and outlook. Oxid Met. 2021;96(5):385. https://doi.org/10.1007/s11085-021-10033-y.

[2] Long HB, Mao SC, Liu YN, Zhang Z, Han XD. Microstructural and compositional design of Ni-based single crystalline superalloys - a review. J Alloy Compd. 2018;743:203. https://doi.org/10.1016/j.jallcom.2018.01.224.

[3] Ye XJ, Yang BB, Nie Y, Yu S, Li YP. Influence of Nb addition on the oxidation behavior of novel Ni-base superalloy. Corros Sci. 2021;185:109436. https://doi.org/10.1016/j.corsci.2021.109436.

[4] Xu F, Le PW, Li HS, Huang AH, Zhang JF, Bao J. High-temperature oxidation behavior and mechanism of second-generation Nickel-based single crystal superalloy. Chin J Rare Met. 2023;47(4):493. https://doi.org/10.13373/j.cnki.cjrm.XY22060006.

[5] Zhai YD, Chen YH, Zhao YS, Long HB, Li XQ, Deng QS, Lu H, Yang XM, Yang G, Li W, Yang LY, Mao SC, Zhang Z, Li A, Han XD. Initial oxidation of Ni-based superalloy and its dynamic microscopic mechanisms: the interface junction initiated outwards oxidation. Acta Mater. 2021;215:116991. https://doi.org/10.1016/j.actamat.2021.116991.

[6] Zhang JL, Zhaoa ZH, Kong YH, Zhang Z, Zhong QP. Crack initiation and propagation mechanisms during thermal fatigue in directionally solidified superalloy DZ125. Int J Fatigue. 2019;119:355. https://doi.org/10.1016/j.ijfatigue.2018.09.001.

[7] Ma JY, Jiang WX, Wang J, Zhang YF, Zhang Z. Initial oxidation behavior of a single crystal superalloy during stress at 1150 °C. Sci Rep. 2020;10(1):3089. https://doi.org/10.1038/s41598-020-59968-3.

[8] Ramsay JD, Evans HE, Child DJ, Taylor MP, Hardy MC. The influence of stress on the oxidation of a Ni-based superalloy. Corros Sci. 2019;154:277. https://doi.org/10.1016/j.corsci.2019.04.023.
[9] Wang HP, Liu D, Wang JG, Yang YH, Wang LX, Wang H, Rao HD, Nan JG. Role of size and amount of γ' phase on creep properties of Waspaloy. Mater Charact. 2021;181:111498. https://doi.org/10.1016/j.matchar.2021.111498.
[10] Yao HX, Dong JX, Gong ZH, Zhao JQ, Yang G. Influence of replacing molybdenum with tungsten on the creep fracture property of waspaloy Nickel-based alloy. Metals. 2022;12(11):1842. https://doi.org/10.3390/met12111842.
[11] Wu S, Song HY, Peng HZ, Hodgson PD, Wang H, Wu XH, Zhu YM, Lam MC, Huang AJ. A microstructure-based creep model for additively manufactured nickel-based superalloys. Acta Mater. 2022;224:117528. https://doi.org/10.1016/j.actamat.2021.117528.
[12] Yildirim CV, Sirin S, Kivak T, Sarikaya M. The effect of nanofluids reinforced with different surfactants on the machining and friction-wear properties of Waspaloy. Tribilogy Int. 2023;181:108316. https://doi.org/10.1016/j.triboint.2023.108316.
[13] Su R, Li JX, Wu DY, Hu FH, Liang XZ, Shen QY, Tian WG, Wang YL, Ma HK, Narayanaswamy B, Dong HC, Wang Q. Microstructural evolution and hot-compressive behavior of Waspaloy forged bolts: experimental and finite element simulation. J Market Res. 2023;24:3194. https://doi.org/10.1016/j.jmrt.2023.03.206.
[14] Yang JJ, Jing FL, Yang ZM, Jiang KH, Hu DY, Zhang B. Thermomechanical fatigue damage mechanism and life assessment of a single crystal Ni-based superalloy. J Alloy Compd. 2021;872:159578. https://doi.org/10.1016/j.jallcom.2021.159578.
[15] Ma WB, Luo HY, Yang XG. The effects of grain size and twins density on high temperature oxidation behavior of nickel-based superalloy GH738. Materials. 2020;13(18):4166. https://doi.org/10.3390/ma13184166.
[16] Wang J, Xue H, Wang Y. Oxidation behavior of Ni-based superalloy GH738 in static air between 800 and 1000 °C. Rare Met. 2021;40(3):616. https://doi.org/10.1007/s12598-020-01513-2.
[17] Zhou CH, Ma HT, Wang L. Comparative study of oxidation kinetics for pure nickel oxidized under tensile and compressive stress. Corros Sci. 2010;52(1):210. https://doi.org/10.1016/j.corsci.2009.09.005.
[18] Ye XJ, Yang BB, Liu JT, Lai RL, Li YP. Influence of minor tensile stress on the oxidation behavior of powder metallurgy superalloy. Corros Sci. 2022;206:110492. https://doi.org/10.1016/j.corsci.2022.110492.
[19] Qi HY, Liang XB, Li SL, Yang XG. High-temperature oxidation behavior of DZ125 Ni-based superalloy under tensile stress. Rare Met. 2022;41(12):4188. https://doi.org/10.1007/s12598-016-0767-7.
[20] Latief FH, Kakehi K, Fu XT, Tashiro Y. Isothermal oxidation behavior characteristics of a second generation Ni-base single crystal superalloy in air at 1000 and 1100 degrees C. Int J Electrochem Sci. 2012;7(9):8369. https://doi.org/10.1016/S1452-3981(23)18000-X.
[21] Zheng L, Zhang MC, Dong JX. Oxidation behavior and mechanism of powder metallurgy Rene95 nickel based superalloy between 800 and 1000 degrees C. Appl Surf Sci. 2010;256(24):7510. https://doi.org/10.1016/j.apsusc.2010.05.098.
[22] Sun XY, Zhang LF, Pan YM, Huang ZW, Jiang L. Investigation of breakaway oxidation kinetics of nickel-base single crystal superalloys: modeling and experiments. Materials Today Communications. 2022;32:103893. https://doi.org/10.1016/j.mtcomm.2022.103893.
[23] Zhang JC, Jia LN, Weng JF, Su LF, Kong B, Zhang H. Microstructures and high-temperature oxidation behavior of directionally solidified Nb–Si-based alloys with Re additions. Rare Met. 2023;42(1):273. https://doi.org/10.1007/s12598-016-0788-2.
[24] Chang JX, Wang D, Zhang G, Lou LH, Zhang J. Interaction of Ta and Cr on Type-I hot corrosion resistance of single crystal Ni-base superalloys. Corros Sci. 2017;117:35. https://doi.org/10.1016/j.corsci.2017.01.011.
[25] Teng JW, Gong XJ, Yang BB, Yu S, Liu JT, Li YP. Influence of Ti addition on oxidation behavior of Ni-Cr-W-based superalloys. Corros Sci. 2021;193:109882. https://doi.org/10.1016/j.corsci.2021.109882.
[26] Stott FH, Wood GC, Golightly FA. The isothermal oxidation behaviour of Fe-Cr-Al and Fe-Cr-Al-Y alloys at 1200°C. Corros Sci. 1979;19(11):869. https://doi.org/10.1016/S0010-938X(79)80110-9.
[27] Moricca MDP, Varma SK. Isothermal oxidation behaviour of Nb–W–Cr Alloys. Corros Sci. 2010;52(9):2964. https://doi.org/10.1016/j.corsci.2010.05.009.
[28] Pei HQ, Li M, Wang P, Yao XH, Wen ZX, Yue ZF. The effect of tensile stress on oxidation behavior of nickel-base single crystal superalloy. Corros Sci. 2021;191:109737. https://doi.org/10.1016/j.corsci.2021.109737.
[29] Jiang H, Dong JX, Zhang MC, Zheng L, Yao ZH. Oxidation behavior and mechanism of Inconel 740H alloy for advanced ultra-supercritical power plants between 1050 and 1170 °C. Oxid Met. 2015;84(1–2):61. https://doi.org/10.1007/s11085-015-9543-6.
[30] Barnard BR, Liaw PK, Buchanan RA, Klarstrom DL. Affects of applied stresses on the isothermal and cyclic high-temperature oxidation behavior of superalloys. Mater Sci Eng, A. 2010;527(16–17):3813. https://doi.org/10.1016/j.msea.2010.03.050.